Neutron scattering study of tantalum dihydride

Mikhail A. Kuzovnikov,[1,*] Vladimir E. Antonov,[1] Alexandre S. Ivanov,[2] Thomas Hansen,[2] Stanislav Savvin,[2] Valery I. Kulakov,[1] Marek Tkacz,[3] Alexander I. Kolesnikov,[4] and Vladislav M. Gurev[1,5]

[1]*Institute of Solid State Physics RAS, 142432 Chernogolovka, Moscow District, Russia*
[2]*Institut Laue-Langevin, 71 Avenue des Martyrs CS 20156, 38042 Grenoble Cedex 9, France*
[3]*Institute of Physical Chemistry PAS, 44/52 Kasprzaka, 01–224 Warsaw, Poland*
[4]*Neutron Scattering Division, Oak Ridge National Laboratory, Oak Ridge, Tennessee 37831, USA*
[5]*Moscow State University, 119992 Moscow, Russia*

(Received 13 January 2020; revised 6 July 2020; accepted 15 July 2020; published 31 July 2020)

A single-phase sample of $TaH_{2.2(1)}$ with a hexagonal close-packed metal lattice (hcp; space group $P6_3/mmc$) was synthesized under a hydrogen pressure of 9 GPa and a temperature of 100 °C; quenched to the liquid nitrogen temperature; recovered to ambient pressure and studied by neutron diffraction (ND) and inelastic neutron scattering (INS). The ND study showed that hydrogen atoms occupied one half of the tetrahedral (T) and all octahedral (O) interstitial sites in the hcp lattice of Ta atoms. The arrangement of the H atoms over the T sites was proven to be ordered, which lowered the symmetry of the full crystal structure of the dihydride to $P6_3mc$. Due to the resulting asymmetry in the local environment of the O sites, the H atoms were considerably displaced from the centers of these sites along the z axis, away from the H atoms occupying the neighboring T sites. The INS study demonstrated that the potential wells for H atoms at both the T and O sites are highly anharmonic and anisotropic. The potential wells at the O sites are softer along the z axis than in the x, y plane, while the T sites show opposite anisotropy.

DOI: 10.1103/PhysRevB.102.024113

I. INTRODUCTION

Hydrides of transition metals attract the attention of many researchers due to their unusual physical properties and important technical applications as hydrogen and energy storage materials. Particularly, after the discovery of superconductivity with a critical temperature of $T_c \approx 200$ K in the H_3S compound with a body-centered cubic (bcc) sulfur lattice at a pressure of ∼150 GPa [1,2], similar or higher superconducting temperatures were predicted for high-pressure metal hydrides with extremely large H-to-metal ratios [3]. This triggered intensive experimental studies at the utmost hydrogen pressures in diamond anvil cells, which led to the synthesis of multiple new metal hydrides with a very high hydrogen content (such as $cI16$-NbH_3 [4], $I4/mmm$-FeH_5 [5], LaH_{10} with a face-centered cubic (fcc) metal lattice [6] and many others). Moreover, the fcc-LaH_{10} "superhydride" was shown to have a record $T_c \approx 250$ K at 170 GPa [7,8] in fair agreement with the theoretical predictions [3,9].

The main difficulty in the synthesis and studies of new hydrogen-rich materials is the need to compress gaseous hydrogen to ultrahigh pressures, which constrains the list of properties that can be studied. For most new hydrides synthesized in diamond anvil cells, only the crystal structure of the metal lattice was experimentally determined using *in situ* x-ray diffraction. The hydrogen content of any new hydride has not been determined experimentally yet, not to say about the full crystal structure and the vibrational spectrum, which could only be examined with neutron scattering techniques. As a rule, the hydrogen content of the new hydride and the positions of H atoms in its metal lattice are predicted using *ab initio* calculations, and then the predictions are verified by comparison with the experimentally measured baric dependences of the atomic volume. The results of the comparison can only be considered as preliminary, because of the systematic volume overestimation inherent in the most popular calculation methods involving generalized-gradient-approximation-based density functionals, and because of the inability of these methods to take into account the possible nonstoichiometric composition of the hydride.

Most high-pressure hydrides ever studied by neutron diffraction (ND) and inelastic neutron scattering (INS) were synthesized in the amounts of a few hundred milligrams using large-volume Toroid-type high-pressure chambers, quenched to the liquid N_2 temperature and investigated *ex situ* in a metastable state at ambient pressure [10]. In view of the relatively low hydrogen pressures up to 9–10 GPa achievable with these apparatuses, the last of those hydrides, CoH with a face-centered cubic (fcc) metal lattice, was synthesized and studied by ND and INS more than a decade ago [11]. It was only recently that we synthesized a massive sample of a new binary high-pressure dihydride, $TaH_{2.2}$ [12]. This dihydride was formed from the low-pressure substoichiometric tantalum monohydride at H_2 pressures above 5.5 GPa, and a 24 h exposure to a pressure of 9 GPa at 150 °C proved to be sufficient to produce single-phase, homogeneous samples suitable for the studies by the methods of neutron physics.

A neutron diffraction investigation of tantalum dihydride was of prime interest because of its hcp metal lattice, which

*Corresponding author: kuz@issp.ac.ru

is not typical of dihydrides of *d* metals. At present, $TaH_{2.2}$ is one of only three such dihydrides obtained in experiment. The other two are hcp-CrH_2 [13] and hcp-NbH_2 [4]; however, both these dihydrides are formed at hydrogen pressures above 30–40 GPa that makes their neutron diffraction studies very unlikely in the foreseeable future. Therefore, $TaH_{2.2}$ provides the unique opportunity for the ND investigation of the full crystal structure of an hcp dihydride of a *d* metal.

In contrast to the simple crystal structures of low-pressure dihydrides with the fcc metal lattices (those of Ti, Zr, Hf, V, and Nb), in which H atoms just fill all tetrahedral interstitial sites [14], the formation of a dihydride on the basis of an hcp metal lattice requires a more complicated distribution of H atoms over both the T and O sites. The reason is that the T sites in the hcp lattice form close-spaced pairs. In the hcp-$TaH_{\sim 2}$, the distance between the centers of T sites in each pair is about 1.3 Å. At the same time, the minimal distance between hydrogen atoms cannot be much less than 2 Å in any transition metal [15]. Due to this "blocking effect", only one T site in a pair can be occupied by a hydrogen atom in the tantalum dihydride. Since the number of T sites in the hcp metal lattice is twice as large as the number of metal atoms and the number of O sites is equal to the number of metal atoms, one half of the H atoms in TaH_2 should therefore sit on the T sites and another half on the O sites.

In the presence of strong H-H interaction, a long-range order can develop in the arrangement of hydrogen atoms among the T sites that will lead to lowering the symmetry of the crystal. The simplest scenarios are the formation of a $P6_3mc$ structure (only the T site with the lower *z* coordinate is occupied in each pair) and a *Pnma* structure (cell doubling). The latter is also called a cotunnite-type structure. *Ab initio* calculations predicted [16] that the hydrogen sublattice in hcp-TaH_2 should be ordered at $T = 0$ K and form a $P6_3mc$ structure at pressures below 90 GPa, and a *Pnma* (cotunnite-type) structure at higher pressures. For comparison: similar calculations predicted a *Pnma* structure for hcp-CrH_2 [13,17] and a $P6_3mc$ structure for hcp-NbH_2 [18].

The hcp metal lattice is typical of dihydrides of alkaline-earth metals, namely BaH_2, SrH_2, CaH_2, and an "HP2" high-pressure phase of MgH_2 [19]. Dihydrides of rare earths have fcc metal lattices, with the exception of hcp-EuH_2 and hcp-YbH_2. In all these hcp dihydrides, one half of the H atoms fills the O sites, while the other half occupies the T sites and invariably forms an ordered *Pnma* (cotunnite-type) structure. Under a sufficiently high pressure, each pair of T sites in CaH_2 and SrH_2 [20], BaH_2 [21], EuH_2 [22], YbH_2 [23], and YbD_2 [24] merges into one site with a planar triangular coordination producing a Ni_2In-type structure. This structure belongs to the $P6_3/mmc$ space group, which is a common supergroup of both *Pnma* and $P6_3mc$ ordering scenarios. The $P6_3mc$ structure has not been observed in any dihydride yet.

The predicted positional ordering in the H sublattice of the hcp tantalum dihydride should strongly affect its spectrum of optical hydrogen vibrations. The most effective tool for studying these vibrations is inelastic neutron scattering because neutrons in the tantalum dihydride predominantly scatter on the H atoms due to their large incoherent neutron scattering cross section and small mass compared to the Ta atoms.

In the present paper, a $TaH_{2.2}$ powder sample weighing 325 mg was prepared in a series of a few high-pressure syntheses and studied by both the ND and INS methods. We must admit that $TaD_{2.2}$ would be more suitable for the ND investigation due to the small incoherent neutron scattering cross section of the D atoms, but we failed to produce tantalum dideuteride at our maximal D_2 pressure of 9 GPa. It can also be mentioned that the ND investigation of $TaH_{2.2}$ was necessary anyway for a more reliable interpretation of the INS results, because crystal structures of a hydride and deuteride of the same metal can significantly differ (for example, different phases appear in phase diagrams of the V-H and V-D systems [25]).

II. EXPERIMENTAL DETAILS

The single-phase powder sample of tantalum dihydride with the total weight of 325 mg was collected of a few separately synthesized samples weighing 30–70 mg each and prepared by the same method as the samples in our previous work [12]. Namely, plates of a 99.9% Ta foil with a thickness of 0.16 mm and total weight of 50–100 mg were loaded with hydrogen by a 48 h exposure to a hydrogen atmosphere at 9 GPa and 100 °C in a Toroid-type high-pressure chamber [26] using NH_3BH_3 as an internal hydrogen source [27]. After the hydrogenation was completed, the sample was cooled together with the chamber to the liquid N_2 temperature; the pressure was released, the chamber was disassembled under liquid nitrogen, and the sample was recovered from the chamber and further stored in liquid nitrogen in order to prevent hydrogen losses.

Each hydrogenated sample was then examined by x-ray diffraction at 85 K to ensure that it was a single-phase hcp tantalum dihydride; the detection limit of possible TaH or Ta impurities was about 3%. The hydrogen content of the samples was determined by hot extraction of the hydrogen into a pre-evacuated calibrated volume in the regime of heating the sample from −186 to 650 °C at a rate of 10 °C min^{-1} [28]. The mass of the analyzed probe was a few milligrams; the accuracy in determining the atomic ratio H/Ta was 3%. Taking into account all the uncertainties, the hydrogen content of tantalum dihydride was determined with an accuracy of 5% and was equal to H/Ta = 2.2(1). The hydrogenated plates were brittle. Prior to the neutron scattering experiments, they were all assembled together and ground in an agate mortar under liquid nitrogen to reduce texture effects.

The powder $TaH_{2.2}$ sample thus prepared was studied by neutron diffraction at $T = 100$ K with the high-luminosity D20 instrument at the Institute Laue-Langevin in Grenoble using a Ge(117) monochromator with vertical focussing in the high resolution configuration [29]. The monochromator takeoff angle of 118° was used to select neutrons with a wavelength of 1.358 Å, as determined from a Rietveld analysis of the diffraction pattern of a $Na_2Ca_3Al_2F_{14}$ standard measured separately. While still in liquid nitrogen, the powdered $TaH_{2.2}$ sample was wrapped in thin aluminum foil and placed into a standard vanadium holder with an inner diameter of 5 mm. Unwanted parts of the sample holder were masked with cadmium foil, which produced some weak sharp peaks at large angles of $2\theta > 140°$. The data acquisition time was

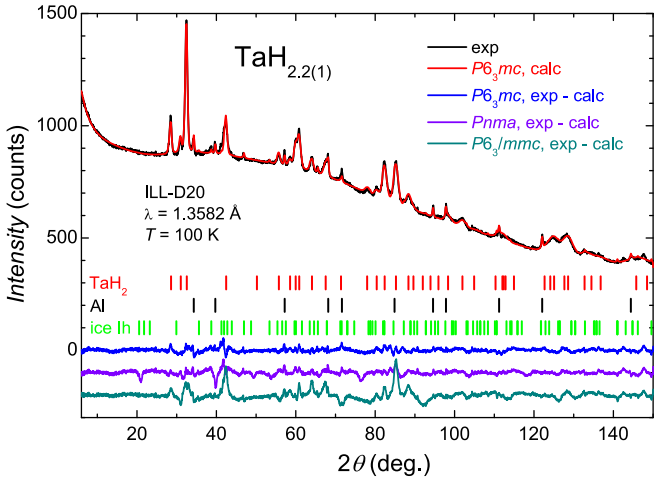

FIG. 1. Neutron powder diffraction pattern of the hcp-$TaH_{2.2}$ sample (black curve) measured at $T = 100$ K with the D20 instrument at ILL, Grenoble, and the results of its profile analysis using three structural models with fully occupied O sites and different arrangements of H atoms on the half-occupied T sites. The refined structural parameters are listed in Table I.

6 h. Rietveld refinements were done with the FULLPROF 7.00 program.

Inelastic neutron scattering was studied on the same $TaH_{2.2}$ sample at $T = 10$ K with the IN1-Lagrange inverted geometry spectrometer installed at the hot source of the high-flux reactor at ILL [30]. The energy E_i of the incoming neutrons was selected in the range 27–450 meV with a Cu(220) monochromator with a horizontal and vertical focusing. The average neutron scattering angle on the sample was 90°. The average neutron energy after passing the pyrolytic graphite analyzer was fixed at $E_f = E_i - E = 4.5$ meV, where E is the neutron energy transfer. The energy resolution of the spectrometer was $\delta E/E \approx 3\%$. A background from the cryostat without the $TaH_{2.2}$ sample, but with the sample holder made of aluminum foil and the water ice condensed on it while loading the sample, was measured separately under the same conditions and subtracted from the experimental INS spectrum. The resulting spectrum was normalized to the constant neutron flux at the sample.

The vibrational properties of TaH_2 were calculated by density-functional theory using a plane-wave pseudopotential method as implemented in the CASTEP code [31,32]. We used ultrasoft pseudopotentials with a plane-wave cutoff of 300 eV and the Perdew-Burke-Ernzerhof approximation for exchange and correlation. Phonon calculations were performed within the finite displacement approach with the supercells defined by a cutoff radius of 5 Å [31].

III. RESULTS AND DISCUSSION

A. Neutron diffraction

The neutron powder diffraction pattern of the hcp-$TaH_{2.2}$ sample measured with the D20 instrument at ILL is shown by the black curve in Fig. 1. The intense "background" resulting from the strong incoherent neutron scattering by the H atoms considerably degrades the statistical accuracy of the experiment and precludes from a systematic analysis of subtle effects, such as the distribution of the "overstoichiometric" 0.2 atom H per formula unit in the hcp Ta lattice. Accordingly, we started with determining the presence and type of hydrogen ordering at the T sites assuming the stoichiometric composition TaH_2 of the dihydride. Based on the theoretical predictions [16], we performed Rietveld refinements for the $P6_3mc$ and *Pnma* ordered structural models and also examined the applicability of the completely disordered $P6_3/mmc$ model.

To be able to compare the qualities of the profile fits, we had to do each calculation with the same set of refinable parameters. It was found that with the disordered $P6_3/mmc$ model, the occupancies and atomic thermal parameters converged to unphysical values, so we decided to fix these parameters in all three models. The calculated best fit pattern for the $P6_3mc$ model is shown in Fig. 1 by the red curve, and the refinement residuals for all three models are presented at the bottom of this figure. The resulting structural parameters are listed in Table I. Schematic images of the model crystal structures used in the refinements are shown in Fig. 2.

As seen from Table I and the residual curves in Fig. 1, the $P6_3/mmc$ model assuming a random filling of half of the T sites with the H atoms is fully inconsistent with the experiment. In agreement with the theoretical predictions [16], the order in the arrangement of H atoms at the T sites is

TABLE I. Refined parameters of three different structural models for the composition TaH(octa)H(tetra), corresponding to a different ordering of hydrogen atoms in tetrasites. All refinements were carried out with the same set of refinable parameters, which included the profile functions, instrumental parameters, background, and absorption correction. The atomic thermal parameters and site occupancies had fixed values of $B_{iso} = 0$ and $w = 1$ or 1/2, respectively. The refinement residuals for each model are shown at the bottom of Fig. 1.

Model	Atom	Wyckoff position	x	y	z	w (fixed)	R_p, %	R_{wp},%
$P6_3/mmc$ (No. 194)	Ta	2c	1/3	2/3	1/4	1	1.77	2.82
with disordered H(tetra)	H(octa)	2a	0	0	0	1		
$a = 3.221$ Å; $c = 5.131$ Å	H(tetra)	4f	1/3	2/3	0.667(10)	0.5		
$P6_3mc$ (No. 186)	Ta	2b	1/3	2/3	1/4	1	0.88	1.17
$a = 3.223$ Å; $c = 5.143$ Å	H(octa)	2a	0	0	0.882(5)	1		
	H(tetra)	2b	1/3	2/3	0.631(5)	1		
Pnma (No. 62, cotunnite)	Ta	4c	0.755(5)	1/4	0.075(5)	1	1.03	1.45
$a = 5.139$ Å; $b = 3.222$ Å;	H(octa)	4c	0.334(5)	1/4	0.786(5)	1		
$c = 5.581$ Å	H(tetra)	4c	0.386(5)	1/4	0.115(5)	1		

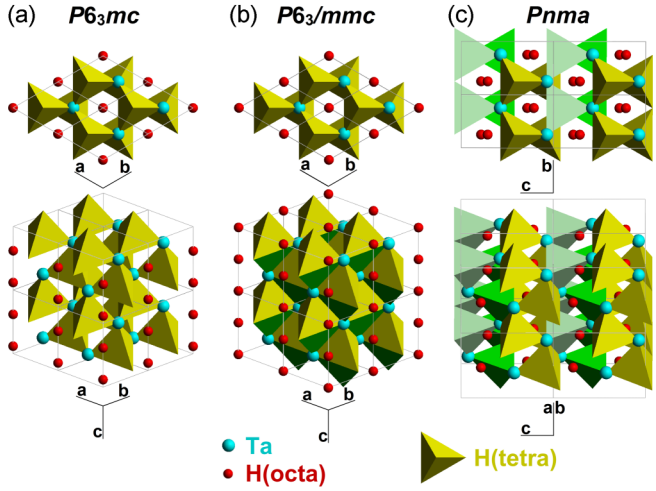

FIG. 2. Three models of the arrangement of hydrogen atoms in the octahedral (O) and tetrahedral (T) interstitial sites of the hcp metal lattice of TaH_2. The Ta and H(octa) atoms are shown with large cyan and small red spheres, respectively; the tetrahedra show the T sites occupied by the H(tetra) atoms. In each model, shown in two projections, H atoms fill all the O sites and one half of the T sites. (a) The ordered $P6_3mc$ model, in which H(tetra) atoms fill only the T sites with the lower z coordinate. The H(octa) and H(tetra) atoms are displaced from the centers of the corresponding interstices by $-0.12c$ and $+0.006c$, respectively, along the z axis. (b) The disordered $P6_3/mmc$ model, in which H(tetra) atoms are randomly distributed among all available T sites with equal probability. (c) The ordered *Pnma* model also known as a cotunnite-type structure. The H atoms are all displaced from the centers of interstices in the hcp tantalum lattice and form an orthorhombic sublattice. The refined lattice parameters and atomic coordinates for the three models are listed in Table I.

better represented by the $P6_3mc$ model compared to the *Pnma* one. Therefore, further we will only rely on the $P6_3mc$ model of the crystal structure of TaH_2.

As can also be seen from Table I, the H(octa) atoms are significantly displaced by $0.12c \approx 0.6$ Å from the centers of the T sites along the z axis in the direction opposite to the nearest neighboring H(tetra) atoms. The displacement increases the shortest H–H interatomic distance from about 2.0 to about 2.3 Å, which excludes any "blocking effect" [15] for H atoms at the T and O sites. The H(tetra) atoms are also displaced from the centers of the T sites along the z axis away from the nearest H(octa) atoms (see Table I), but the displacement is much smaller and only amounts to $0.006c \approx 0.03$ Å.

In order to locate the "overstoichiometric" hydrogen $\delta(\mathrm{H/Ta}) = 0.2$ in the metal lattice of $TaH_{2.2}$, we carried out two additional refinements with the $P6_3mc$ model including the occupancies and atomic thermal parameters as refinable variables: (i) H atoms were only allowed on the O and T sites of the perfectly ordered $P6_3mc$ structure [16]; (ii) H atoms could also randomly occupy the alternative T sites designated as H(tetra2) positions. In both models, the occupancy of the sites of each type was refined as a free parameter.

Results of the fits with and without H(tetra2) atoms are given in Table II. As one can see, the increase in the number of refined parameters did not significantly improve the residual R factors compared with the stochiometric $P6_3mc$ model. Thus, the statistical accuracy of the measured ND pattern proved to be insufficient to locate the "overstoichiometric" hydrogen atoms in the crystal structure of $TaH_{2.2}$. This problem might be solved in the future if one prepares a massive sample of tantalum dideuteride that will exclude the anomalously intense incoherent neutron scattering by H atoms.

TABLE II. Refined parameters of two $P6_3mc$ structural models with variable occupancies w and atomic thermal parameters B_{iso}. The lattice parameters are $a = 3.223$ Å and $c = 5.143$ Å in both models. In the schematic diagrams in the leftmost column, Ta atoms are shown in cyan; H(octa) are red, and H(tetra) and H(tetra2) are green and blue, respectively. The shortest H-H interatomic distances are indicated in Angstroms.

Composition and schematic image	Atom	Wyckoff position	x	y	z	B_{iso}, Å^2	w	R_p, %	R_{wp},%
$TaH_{1.96}$	Ta	2b	1/3	2/3	1/4	0.12(5)	1		
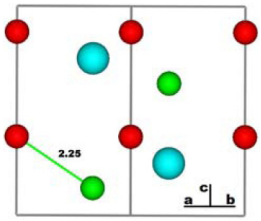	H(octa)	2a	0	0	0.876(10)	0.66(10)	0.99(3)	0.85	1.13
	H(tetra)	2b	1/3	2/3	0.631(5)	0.45(10)	0.96(4)		
$TaH_{2.34}$	Ta	2b	1/3	2/3	1/4	0.12(5)	1		
	H(octa)	2a	0	0	0.874(5)	0.67(10)	1.17(4)		
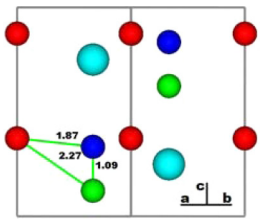	H(tetra)	2b	1/3	2/3	0.623(10)	1.2(2)	0.87(3)	0.83	1.10
	H(tetra2)	2b	1/3	2/3	0.83(2)	0(fixed)	0.29(4)		

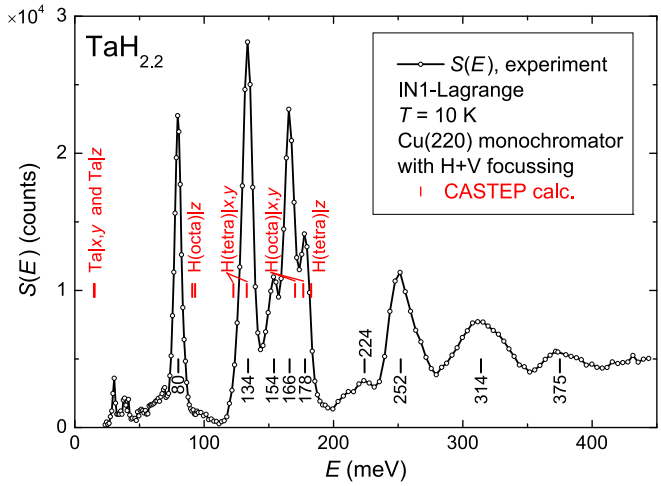

FIG. 3. The dynamical structure factor $S(E)$ of the powder $TaH_{2.2}$ sample as a function of the neutron energy loss E measured at $T = 10$ K with the IN1-Lagrange spectrometer at ILL, Grenoble. The spurious intensity below 50 meV resulted from the contamination of the incoming neutron beam with $\lambda/2$ neutrons. The bottom row of black tics shows the positions of the experimental peaks indicated in Table IV. The upper row of red ticks with red labels shows the energies and polarizations of vibrational modes at the Γ point of the Brillouin zone of $P6_3mc$-TaH_2 resulted from *ab initio* calculations and presented in Table III. All calculated modes with the *x,y* polarization are twice degenerate, while the *z*-polarized modes are nondegenerate.

B. Inelastic neutron scattering

Figure 3 presents the experimental INS spectrum of $TaH_{2.2}$ after subtracting the background from the cryostat and aluminum sample holder and a proper normalization to the constant neutron flux. Due to the large incoherent cross section and small atomic mass of hydrogen compared to tantalum, the spectrum represents nearly exclusively the neutron scattering by the hydrogen atoms.

To assign the peaks in the spectrum to the specific vibrations of H atoms, we performed *ab initio* calculations of phonons at the Γ point in stoichiometric TaH_2 using the $P6_3mc$ structural model discussed above. An analysis of the phonon eigenvectors showed that the vibrations of the H(octa) and H(tetra) atoms are not independent, and there is always a small but noticeable (about 15%) contribution of the vibrations of atoms of one type to the vibrations of atoms of another type. In this paper, the calculated modes are named according to the type of the atoms whose contribution is dominant. For symmetry reasons, all modes at the Γ point have a definite polarization, either in the *x,y* plane or along the *z* axis, which simplified the analysis. The results of the calculation are presented in Table III and in Fig. 3.

The first peak at 80 meV can undoubtedly be assigned to the vibration of H(octa) atom along the *z* axis. A two-phonon scattering process from this vibration can be expected at a neutron energy transfer of about $2 \times 80 = 160$ meV with the intensity lower than that of the 80 meV peak (a detailed intensity calculation of the multiphonon processes will be given later). Such a two-phonon process can be ascribed to the experimental peak at 154 meV. The shift of this peak to the lower energy from its position in the harmonic approximation points to a "soft" anharmonism of the potential well for H(octa) atoms along the *z* axis.

TABLE III. Results of *ab initio* calculations of phonon frequencies and eigenvectors in the Γ point of the Brillouin zone of $P6_3mc$-TaH_2. Note that the E_1 and E_2 modes with the *x,y* polarization are twice degenerate, while the A_1 and B_2 modes with the *z* polarization are nondegenerate. The calculated frequencies $\hbar\omega$ are shown by red ticks in Fig. 3.

Calculated $\hbar\omega$, meV	Irreducible representation	Vibrating atom	Polarization
0	E_1	Acoustic	*x*, *y*
0	A_1	Acoustic	*z*
15	B_2	Ta	*z*
15	E_2	Ta	*x*, *y*
91	A_1	H(octa)	*z*
93	B_2	H(octa)	*z*
123	E_1	H(tetra)	*x*, *y*
133	E_2	H(tetra)	*x*, *y*
170	E_2	H(octa)	*x*, *y*
177	E_1	H(octa)	*x*, *y*
183	A_1	H(tetra)	*z*
183	B_2	H(tetra)	*z*

In the 120–190 meV range, the calculations predict three one-phonon peaks due to the H(tetra)|*x*, *y*, H(octa)|*x*, *y*, and H(tetra)|*z* vibrations listed in the order of increasing frequency. The INS intensity of one-phonon processes being proportional to the generalized phonon density of states, the integral intensity ratios of these peaks should be 2:2:1, which allows us to assign these vibrations to the experimental peaks at 134, 166, and 178 meV, respectively. The resulting mode assignments at $E < 200$ meV are summarized in Table IV. At $E > 200$ meV, all scattering intensity has a multiphonon origin.

As one can see, the potential well for H(octa) in $TaH_{\sim 2}$ is characterized by a strong anisotropy, which manifests itself in the large splitting between the fundamental vibrational frequencies along the *z* axis ($\hbar\omega_z = 80$ meV) and in the *x*, *y* plane ($\hbar\omega_{x,y} = 166$ meV). Note in this connection that the potential well for the H(octa) atom is mostly formed by the six nearest Ta atoms, and this environment has nearly cubic symmetry because the ratio of $c/a = 1.596$ of the hcp Ta lattice of tantalum dihydride is close to the "ideal" value of $(c/a)_{\rm id} = \sqrt{8/3} \approx 1.633$. Therefore, it is the interaction with the nearest H(tetra) atoms, which breaks the cubic symmetry of the potential well at the O sites, pushes H(octa) atoms away from the geometrical center of the octahedral interstices and leads to the strong anisotropy of the H(octa) vibrations.

As seen from Table IV, optical vibrations of the H(tetra) atoms in tantalum dihydride are also anisotropic, but the anisotropy is much weaker and has a different sign, with $\hbar\omega_z/\hbar\omega_{x,y} = 178$ meV/134 meV.

To estimate the anharmonicity of H vibrations at the O and T sites, we performed multiphonon calculations in a harmonic isotropic approximation using the iterative technique [33]. The calculation procedure uses no theory-dependent fitting parameters and consists of finding a self-consistent deconvo-

TABLE IV. Mode assignments for the vibrational spectrum of hydrogen in $TaH_{\sim 2}$. The plausible energy ranges and predominant polarizations (the third column) of the one-phonon bands are based on the *ab initio* calculations for the center of the Brillouin zone (see Table III and the upper row of red tics in Fig. 3). The assignments for the multiphonon bands are derived from the calculations in the harmonic isotropic approximation (see the cyan and magenta curves in Fig. 4) as discussed in the text.

Experimental E, meV	Calculated $\hbar\omega$, meV	Mode assignment
80	91–93[a]	H(octa)$\|z$
134	123–133[a]	H(tetra)$\|x, y$
154	159[b]	Two-phonon $2 \times$ H(octa)$\|z$
166	170–177[a]	H(octa)$\|x, y$
178	183[a]	H(tetra)$\|z$
224	239[b]	Three-phonon $3 \times$ H(octa)$\|z$
252	245[b]	Two-phonon H(octa)$\|x, y \times$ H(octa)$\|z$
	266[b]	$+ 2 \times$ H(tetra)$\|x, y$
314	311[b]	Two-phonon H(tetra)$\|x, y \times$ H(tetra)$\|z$
	330[b]	$+ 2 \times$ H(octa)$\|x, y$
	354[b]	$+ 2 \times$ H(tetra)$\|z$
375	400[b]	Three-phonon $3 \times$ H(tetra)$\|x, y$
	409[b]	$+$H(octa)$\|x, y \times$ H(octa)$\|x, y \times$ H(octa)$\|z$

[a]One-phonon bands.
[b]Multiphonon bands.

lution of the experimental INS spectrum into the sum of one-phonon and multiphonon contribution. For this, it is necessary to know the distribution of the INS intensity over the entire energy range from $E = 0$ to the maximum single-phonon energy $E_{\max}$. A purely multiphonon experimental spectrum at higher energies is not used in the calculations, and its comparison with the calculated spectrum can be used to reveal the presence (or absence) and characteristic features of the anharmonicity of the potential well for hydrogen atoms in higher excited vibrational states. Multiphonon calculations for tantalum dihydride were performed separately for vibrations of the H(octa) and H(tetra) atoms, because in both single-phonon and multiphonon processes, the neutron is only scattered by one H atom located either in the O or T site, and because vibrations of the H(octa) and H(tetra) atoms are weakly interconnected.

To begin with, we corrected the experimental spectrum $S(E)$ at $E < 70$ meV by removing the spurious contribution from the $\lambda/2$ neutrons and adding some acoustic part calculated from first principles and normalized so that the integral intensities $I(\text{acoustic})/I(\text{optic}) = m_{\text{H}}/m_{\text{Ta}}$, where m_{H} and m_{Ta} are the atomic masses of H and Ta, respectively. Neutron scattering on the H(octa) and H(tetra) atoms was assumed to contribute equally to this acoustic part. Then we separated $S(E)$ into energy regions, where the one-phonon neutron scattering was assumed to be purely on the H(octa) atoms ($E = 60 - 90$ meV and 158–172 meV) or H(tetra) atoms ($E = 110 - 145$ meV and 172–192 meV) according to the assignments in Table IV. The multiphonon contribution to $S(E)$ calculated with the upper boundary of the one-phonon spectrum set at $E_{\max} = 192$ meV is shown in Fig. 4.

As seen from Fig. 4, the calculated multiphonon spectrum (red curve) considerably differs from experiment. Meanwhile, similar calculations have earlier accurately reproduced the two- and three-phonon contributions to the $S(E)$ powder spectra of many hcp and fcc hydrides (hcp-CrH, fcc-CrH, hcp-$MnH_{0.86}$, fcc-$MnH_{0.41}$, fcc-CoH, fcc-NiH, and fcc-PdH; see [34] and [35] for references and discussion) and correctly outlined the energy range of the two-phonon band in the anharmonic and anisotropic spectrum of fcc-RhH [35]. Therefore, the poor agreement between the calculated multiphonon scattering intensity and experimental $S(E)$ indicates a strong anharmonicity of the potential well for H atoms in tantalum dihydride.

Nevertheless, some preliminary assignments of certain multiphonon processes to the experimental peaks in the high-energy part of the INS spectrum of $TaH_{\sim 2}$ can be made based on the calculations in the isotropic harmonic

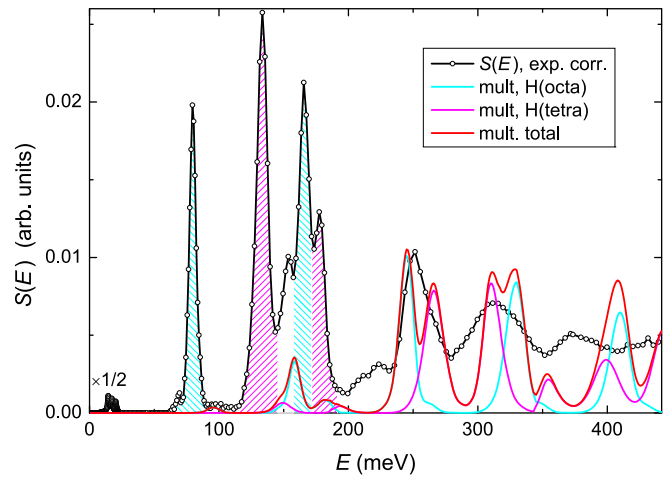

FIG. 4. Corrected dynamical structure factor $S(E)$ of the powder $TaH_{2.2}$ sample (black curve), and estimated contributions from multiphonon neutron scattering on the H(octa) atoms (cyan curve), H(tetra) atoms (magenta curve) and the sum of these contributions (red curve). The fundamental vibrational bands are cross-hatched according to the type of the interstitial site, in which the hydrogen atom vibrates. The positions and polarizations of the calculated multiphonon peaks are listed in Table IV.

approximation. As one can see from Fig. 4 and Table IV, the intensive experimental peak at 252 meV is likely to result from the two-phonon H(octa)$|x,y$ × H(octa)$|z$ and 2 × H(tetra)$|x,y$ processes. The broad and intensive peak at 314 meV can be formed by three other two-phonon processes: H(tetra)$|x$, y × H(tetra)$|z$ and 2 × H(octa)$|x$, y and 2 × H(tetra)$|z$.

As has already been mentioned, the harmonic approximation gives an overestimated value of 159 meV for the energy of the two-phonon 2 × H(octa)$|z$ experimental peak observed at 154 meV. Most of the calculated "harmonic" energies of other multiphonon processes of neutron scattering on the H(octa) and H(tetra) atoms, which form the experimental peaks at 252 and 314 meV, are also overestimated. This suggests a trumpetlike shape of the potential well for both H(octa) and H(tetra) atoms. The effect is also called soft anharmonism: the higher the energy of the excited state, the smaller the energy difference between the consecutive states.

Let us now see what can be said about the experimental peak (or rather the asymmetric hump) at ∼224 meV shown by the black curve in Fig. 4. In view of its low intensity, the peak cannot be considered as one of the highly intensive two-phonon peaks H(octa)$|x,y$ × H(octa)$|z$ or 2 × H(tetra)$|x,y$ shifted to lower energies due to the soft anharmonicity of the potential well. However, as one can see from the last column of Table IV, the INS spectrum additionally contains a three-phonon 3 × H(octa)$|z$ peak at 239 meV, overlapping with the H(octa)$|x,y$ × H(octa)$|z$ peak. The 3 × H(octa)$|z$ peak has a low intensity because of its three-phonon origin and can be attributed to the broad experimental feature with a maximum at ∼224 meV.

Another contribution to the broad low-energy shoulder of the 224 meV peak can come from the weak "mixed" excitation process H(tetra)$|x$, y × H(octa)$|z$ resulting from a certain (up to 15%) involvement of the H(octa) atoms to the H(tetra)$|x$, y vibration and vice versa, which was neglected in our multiphonon calculations. This two-phonon process will give rise to a peak at E(H(tetra)$|x$, y) + E(H(octa)$|z$) = 134 + 80 = 214 meV in the INS spectrum.

Taking into account the anharmonicity of the experimental $S(E)$ spectrum of tantalum dihydride and the likelihood of the mixed scattering processes, an analysis of the rather featureless intensity distribution at E > 350 meV looks premature. In Table IV, the assignment of the three-phonon 3 × H(tetra)$|x$, y and H(octa)$|x$, y × H(octa)$|x$, y × H(octa)$|z$ processes to the 375 meV peak can only be considered as tentative.

Previously, trumpetlike "soft" anharmonism was observed by INS in $TaH_{\sim 0.1}$ [36,37], $TaD_{0.14}$ [36] and $TaH_{0.71}$ [38], in which H (or D) atoms filled tetrahedral sites in a distorted bcc lattice of Ta metal. Together with our findings for hcp-$TaH_{2.2}$, this suggests that anharmonism of optical hydrogen vibrations is an intrinsic feature of tantalum hydrides.

IV. CONCLUSIONS

This is for the first time that one of many crystal structures of new high-pressure hydrides, predicted by *ab initio* calculations in the recent years, has been examined by neutron diffraction. The fact that experiment confirmed the $P6_3mc$ structure calculated for the hcp tantalum dihydride [16] is encouraging because it gives hope that the predicted structures of the hydrogen sublattices of many other new hydrides formed at very high pressures are also true, although this cannot be verified experimentally yet.

Inelastic neutron scattering demonstrated strong anisotropy and anharmonism of hydrogen optical vibrations on both T and O sites in the hcp metal lattice of $TaH_{2.2}$. The anisotropy of the vibrations was rather well reproduced in our *ab initio* calculations, so that each vibrational band was identified. The anisotropy in the H vibrations on the O sites is likely to be due to the large displacement of the H(octa) atoms from the center of the octahedral interstices caused by the interaction with the H(tetra) atoms asymmetrically occupying one half of the nearest T sites.

ACKNOWLEDGMENTS

The work was partly supported by the Russian Foundation for Basic Research under Grant No. 17-02-01142. A.I.K. acknowledges the support by the Scientific User Facilities Division, Office of Basic Energy Sciences, US Department of Energy.

[1] A. P. Drozdov, M. I. Eremets, I. A. Troyan, V. Ksenofontov, and S. I. Shylin, Nature (London) **525**, 73 (2015).
[2] M. Einaga, M. Sakata, T. Ishikawa, K. Shimizu, M. I. Eremets, A. P. Drozdov, I. A. Troyan, N. Hirao, and Y. Ohishi, Nat. Phys. **12**, 835 (2016).
[3] H. Liu, I. I. Naumov, R. Hoffmann, N. W. Ashcroft, and R. J. Hemley, Proc. Natl. Acad. Sci. USA **114**, 6990 (2017).
[4] G. Liu, S. Besedin, A. Irodova, H. Liu, G. Gao, M. Eremets, X. Wang, and Y. Ma, Phys. Rev. B **95**, 104110 (2017).
[5] C.M. Pépin, G. Geneste, A. Dewaele, M. Mezouar, and P. Loubeyre, Science **357**, 382 (2017).
[6] Z. M. Geballe, H. Liu, A. K. Mishra, M. Ahart, M. Somayazulu, Y. Meng, M. Baldini, and R. J. Hemley, Angew. Chem. Int. Ed. **57**, 688 (2018).
[7] A. P. Drozdov, P. P. Kong, V. S. Minkov, S. P. Besedin, M. A. Kuzovnikov, S. Mozaffari, L. Balicas, F. Balakirev, D. Graf, V. B. Prakapenka, E. Greenberg, D. A. Knyazev, M. Tkacz, and M. I. Eremets, Nature (London) **569**, 528 (2019).
[8] M. Somayazulu, M. Ahart, A. K. Mishra, Z. M. Geballe, M. Baldini, Y. Meng, V. V. Struzhkin, and R. J. Hemley, Phys. Rev. Lett. **122**, 027001 (2019).
[9] F. Peng, Y. Sun, C. J. Pickard, R. J. Needs, Q. Wu, and Y. Ma, Phys. Rev. Lett. **119**, 107001 (2017).
[10] V. E. Antonov, J. Alloys Compd. **330–332**, 110 (2002).
[11] V. E. Antonov, T. E. Antonova, V. K. Fedotov, T. Hansen, A. S. Ivanov, and A. I. Kolesnikov, J. Alloys Compd. **404–406**, 73 (2005).
[12] M. A. Kuzovnikov, M. Tkacz, H. Meng, D. I. Kapustin, and V. I. Kulakov, Phys. Rev. B **96**, 134120 (2017).

[13] A. Marizy, G. Geneste, P. Loubeyre, B. Guigue, and G. Garbarino, Phys. Rev. B **97**, 184103 (2018).
[14] Y. Fukai, *The Metal-Hydrogen System* (Springer, Berlin, 2005).
[15] A. C. Switendick, Electronic structure of transition metal hydrides, in *Transition Metal Hydrides*, edited by R. Bau, Adv. Chem. Ser. Vol. 167 (ACS, Washington, D. C., 1978), pp.264–282.
[16] Q. Zhuang, X. Jin, T. Cui, Y. Ma, Q. Lv, Y. Li, H. Zhang, X. Meng, and K. Bao, Inorg. Chem. **56**, 3901 (2017).
[17] S. Yu, X. Jia, G. Frapper, D. Li, A. R. Oganov, Q. Zeng, and L. Zhang, Sci. Rep. **5**, 17764 (2015).
[18] C. Chen, F. Tian, D. Duan, K. Bao, X. Jin, B. Liu, and T. Cui, J. Chem. Phys. **140**, 114703 (2014).
[19] T. Moriwaki, Yu. Akahama, H. Kawamura, S. Nakano, and K. Takemura, J. Phys. Soc. Jpn. **75**, 074603 (2006).
[20] K. Kinoshita, M. Nishimura, Y. Akahama, and H. Kawamura, in *Proceedings of Joint 20th AIRAPT – 43rd EHPRG International Conference on High Pressure Science and Technology, Karlsruhe*, 2005, edited by E. Dinjus (Karlsruhe Institute of Technology, Karlsruhe, Germany, 2005), p. 276.
[21] K. Kinoshita, M. Nishimura, Y. Akahama, and H. Kawamura, Solid State Commun. **141**, 69 (2007).
[22] T. Matsuoka, H. Fujihisa, N. Hirao, Y. Ohishi, T. Mitsui, R. Masuda, M. Seto, Y. Yoda, K. Shimizu, A. Machida, and K. Aoki, Phys. Rev. Lett. **107**, 025501 (2011).
[23] J. S. Olsen, B. Buras, L. Gerward, B. Johansson, B. Lebech, H. L. Skriver, and S. Steenstrup, Phys. Scr. **29**, 503 (1984).
[24] S. Klotz, M. Casula, K. Komatsu, S. Machida, and T. Hattori, Phys. Rev. B **100**, 020101(R) (2019).
[25] W. Pesch, T. Schober, and H. Wenzl, Scr. Metall. **16**, 307 (1982).
[26] L. G. Khvostantsev, V. N. Slesarev, and V. V. Brazhkin, High Pressure Res. **24**, 371 (2004).
[27] V. E. Antonov, B. M. Bulychev, V. K. Fedotov, D. I. Kapustin, V. I. Kulakov, and I. A. Sholin, Int. J. Hydrogen Energy **42**, 22454 (2017).
[28] I. O. Bashkin, V. E. Antonov, A. V. Bazhenov, I. K. Bdikin, D. N. Borisenko, E. P. Krinichnaya, A. P. Moravsky, A. I. Harkunov, Yu. M. Shul'ga, Yu. A. Ossipyan, and E. G. Ponyatovsky, JETP Lett. **79**, 226 (2004).
[29] M. Kuzovnikov, A. Ivanov, S. Savvin, and M. Tkacz, Crystal structure of novel tantalum hydrides. Institut Laue-Langevin (ILL), doi:10.5291/ILL-DATA.5-22-769 (2019).
[30] M. Kuzovnikov, A. Ivanov, and M. Tkacz, Vibrational dynamics of novel tantalum hydrides. Institut Laue-Langevin (ILL), doi:10.5291/ILL-DATA.7-01-487 (2019).
[31] S. J. Clark, M. D. Segall, C. J. Pickard, P. J. Hasnip, M. I. J. Probert, K. Refson, and M. C. Payne, Z. Kristallogr. **220**, 567 (2005).
[32] K. Refson, P. R. Tulip, and S. J. Clark, Phys. Rev. B **73**, 155114 (2006).
[33] V. E. Antonov, I. T. Belash, A. I. Kolesnikov, J. Mayer, I. Natkaniec, E. G. Ponyatovskii, and V. K. Fedotov, Sov. Phys. Solid State **33**, 87 (1991).
[34] V. E. Antonov, K. Cornell, B. Dorner, V. K. Fedotov, G. Grosse, A. I. Kolesnikov, F. E. Wagner, and H. Wipf, Solid State Commun. **113**, 569 (2000).
[35] V. E. Antonov, T. E. Antonova, V. K. Fedotov, B. A. Gnesin, A. S. Ivanov, and A. I. Kolesnikov, J. Alloys Compd. **446–447**, 508 (2007).
[36] R. Hempelmann, D. Richter, and A. Kollmar, Z. Phys. B **44**, 159 (1981).
[37] S. Ikeda and N. Watanabe, J. Phys. Soc. Jpn. **56**, 565 (1987).
[38] J. Eckert, J. A. Goldstone, D. Tonks, and D. Richter, Phys. Rev. B **27**, 1980 (1983).